Ice Age Paleotopography

W. Richard Peltier

Science, New Series, Vol. 265, No. 5169. (Jul. 8, 1994), pp. 195-201.

Stable URL:
http://links.jstor.org/sici?sici=0036-8075%2819940708%293%3A265%3A5169%3C195%3AIAP%3E2.0.CO%3B2-P

Science is currently published by American Association for the Advancement of Science.

Ice Age Paleotopography

W. Richard Peltier

A gravitationally self-consistent theory of postglacial relative sea level change is used to infer the variation of surface ice and water cover since the Last Glacial Maximum (LGM). The results show that LGM ice volume was approximately 35 percent lower than suggested by the CLIMAP reconstruction and the maximum heights of the main Laurentian and Fennoscandian ice complexes are inferred to have been commensurately lower with respect to sea level. Use of these Ice Age boundary conditions in atmospheric general circulation models will yield climates that differ significantly from those previously inferred on the basis of the CLIMAP data set.

In the reconstruction of climates of the distant past using atmospheric general circulation models [AGCMs; for example, (*1*)], the primary determinant of the quality of the reconstruction is clearly the reliability of the boundary conditions to which the model is subject. In general, the further into the past the epoch chosen as target for analysis, the less reliable will be the information on the basis of which the boundary conditions must be inferred. On time scales of tens of millions of years ago, for example, one must accurately account for the rearrangement of the continents (*2*). Even over hundreds of thousands of years, the surface conditions of the planet have undergone substantial modification. Specifically, for the past 900,000 years (*3*) extensive ice complexes over Canada and northwestern Europe have repeatedly advanced and retreated almost cyclically with a characteristic period of approximately 100,000 years (*4*); glaciation typically takes 90,000 years, significantly longer than the deglaciation time scale of 10,000 years. At 21,000 years ago (21 ka) (*5*), the planet was experiencing the full glacial conditions of the Last Glacial Maximum (LGM) and by approximately 7 ka the ice sheets had disappeared, marking the onset of the Holocene (fully modern) epoch of Earth history.

In order to better understand the large-scale causes of variations of planetary climate that have occurred since the LGM, AGCMs are being used to reconstruct past climates for a sequence of target epochs from LGM to present [for example, (*6*)]. Such analyses have all used CLIMAP (*7*, *8*) data to fix the surface boundary conditions of sea surface temperature (SST), extent and albedo of land ice and sea ice, and paleotopography. Although information on both SST (*9*) and land ice extent (*10*) has improved since CLIMAP, these improvements have affected only relatively localized regions. Of the CLIMAP boundary conditions, paleotopography was by far the most poorly constrained, as was clearly recognized by Denton and Hughes (*8*), who provided two alternative glacial reconstructions to the CLIMAP data. These reconstructions, referred to as the Maximum (MAX) and Minimum (MIN) reconstructions, differed significantly: The former comprised a change in ice volume from the LGM to the present equal to an eustatic sea level rise of 163 m; the latter comprised a change equal to an eustatic rise of 127 m. Denton and Hughes based their reconstructions on the assumption that ice sheets at the LGM were in a state of dynamical equilibrium. Application of steady-state ice mechanical equations then led to a prediction of the thickness distribution given the location of the ice sheet margins. Because the main ice sheets were collectively involved in the 100,000-year Ice Age cycle and the system is known not to have occupied the LGM state for longer than about 5000 years, there is clearly an issue as to the validity of the steady-state assumption that is basic to the CLIMAP (*7*) reconstruction. In this article, I use a method for the deconvolution of relative sea level data to assess LGM (and subsequent) paleotopography. These analyses show that even the CLIMAP MIN model estimate of LGM ice sheet volume (and thus topography) is excessive and that the CLIMAP MAX model, which has been the basis for previous paleoclimatological reconstructions, has an excess volume of 55%. Using the topographically self-consistent version of the theory of postglacial relative sea level change, I translate the new ice sheet thickness distributions inferred from the theory into paleotopography. These modified boundary conditions are expected to lead to the prediction of significant shifts in climate from those previously found [in consequence, for example, of dramatic shifts in atmospheric storm tracks] when they are used in AGCM simulations.

The author is in the Department of Physics, University of Toronto, Toronto, Ontario, Canada M5S 1A7.

Topographically Self-Consistent Sea Levels

Over the past 20 years a detailed understanding has been achieved of the manner in which large-scale redistribution of the ice and water load on the Earth's surface, resulting from the melting of LGM ice sheets and the meltwater loading of the ocean basins, deforms the viscoelastic earth (*11*). The best available record of this deformation consists of time series of relative sea level (*rsl*) history based upon the ^{14}C dating of raised and submerged marine shoreline indicators whose heights above or depths below present-day sea level may be accurately measured. Such data provide a high-quality constraint on the dynamical mechanism of glacial isostatic adjustment. The essence of this process is that, because of the long time scale over which the differential ice and water loads are applied, the shape of the Earth is significantly deformed by viscous flow in its interior. Long time series of *rsl* history accurately record this viscous deformation in the form of a record of the time-dependent separation between the sea surface (a globally defined gravitational equipotential called the geoid) and the surface of the solid Earth. Although many other geophysical data related to the process of glacial isostatic adjustment have also come to be understood, such as anomalies in Earth rotation (*12*) and in the gravitational field (*13*), *rsl* data remain the most important because they constitute a relatively complete historical record of the process, unlike observations that pertain only to a single instant of time. I have assembled [for example, (*14*)] more than 400 globally distributed time series of *rsl* histories, the locations of which are shown on Fig. 1. Approximately half of the *rsl* time series are from ice-covered sites, and each of these is characterized by an essentially exponentially decreasing rate of uplift of the land with respect to the sea in the time period since ice retreat [for example, Fig. 2].

Such almost precisely exponential relaxation curves have the form $rsl(t) = A\cdot[\exp((t - t_p)/\tau) - 1]$ where A is the site-dependent amplitude, τ is the site-dependent relaxation time, and $t - t_p$ is the age in years before present. These curves contain information on both the internal rheology of the planet and the space- and time-dependent thickness of the ice load. If the total time-dependent

surface mass load per unit area is $L(\theta,\lambda,t)$ then we may write

$$L(\theta,\lambda,t) = \rho_I I(\theta,\lambda,t) + \rho_w S(\theta,\lambda,t) \quad (1)$$

where ρ_I is the density of ice, ρ_w the density of water, and $I(\theta,\lambda,t)$ is the space- and time-dependent thickness of the continental ice sheets whose melting induces the change of bathymetry (water thickness) $S(\theta,\lambda,t)$. The fact which makes it possible to reconstruct $I(\theta,\lambda,t)$, using $rsl(t) = S(\theta,\lambda,t)$ data from ice-covered sites such as that illustrated on Fig. 2, is that the relaxation time τ is determined almost entirely by internal mantle rheology, whereas the amplitude A is determined almost entirely by the local history of ice sheet thickness $I(\theta,\lambda,t)$ (*16*). Given a theory that enables one to predict such observed $rsl(t)$, it is possible to invert the theory formally to derive separate quantitative estimates for both mantle viscosity and deglaciation history (*16–18*). I focus on the extension to existing theory that is required to infer paleotopography and present a deglaciation history ICE-4G that was derived through application of this extended theory.

Central to the established viscoelastic theory of postglacial *rsl* change is the sea level equation [for example, (*19*)] that predicts *rsl* histories $S(\theta,\lambda,t)$ as solutions to the integral equation

$$S(\theta,\lambda,t) = C(\theta,\lambda,t)\{G(\theta,\lambda,t) - R(\theta,\lambda,t)\}$$

$$= C(\theta,\lambda,t)\left[\int_{-\infty}^{t}\int\int_{\Omega} L(\theta',\lambda',t')\left\{\frac{\phi(\gamma,t-t')}{g} - \Gamma(\gamma,t-t')\right\}d\Omega' dt' + \frac{\Delta\Phi(t)}{g}\right] \quad (2)$$

in which $G(\theta,\lambda,t)$ and $R(\theta,\lambda,t)$ are the dynamic geoid and solid surfaces, respectively, and where $\phi(\gamma,t-t')$ and $\Gamma(\gamma,t-t')$ are respective viscoelastic surface load Green functions for the gravitational potential perturbation and for the radial displacement induced by a point mass load brought up to the surface of the planet at $t = 0$ and instantaneously removed (*11*). The spatial dependence of these Green functions involves only the angular separation γ between source point (θ',λ') and field point (θ,λ), a consequence of an assumption that the internal viscoelastic structure of the planet is a function of radius only. The function $C(\theta,\lambda,t)$ in Eq. 2 is called the "ocean function" and equals unity where there is ocean and zero where there is land, whereas the function $\Delta\Phi(t)$ is defined as

$$\frac{\Delta\Phi(t)}{g} = -\frac{M_I(t)}{\rho_w A_0} - \frac{1}{A_0}\left\langle \int_{-\infty}^{t}\int\int_{\Omega} L(\theta',\lambda',t')\left\{\frac{\theta(\gamma,t-t')}{g} - \Gamma(\gamma,t-t')\right\}d\Omega' dt' \right\rangle \quad (3)$$

This function is fixed by the requirement that the integral of $\rho_w S(\theta,\lambda,t)$ over the global ocean [integration over this region is indicated by the angle brackets in Eq. 3] equal $M_I(t)$, the mass lost by the ice sheets on melting by time t. In all of my earlier

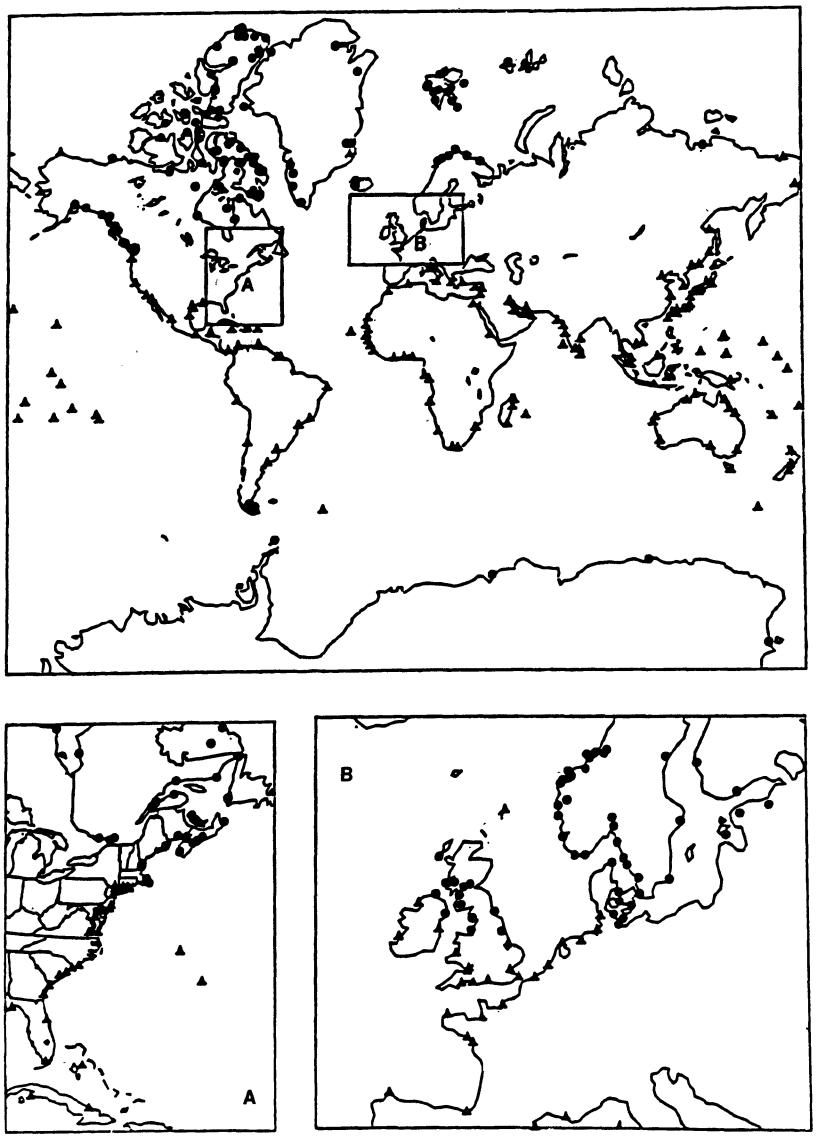

Fig. 1. Location map for ^{14}C-dated relative sea level histories. Sites that were ice covered at LGM are shown as solid circles, whereas sites that were not ice-covered are shown as solid triangles. The data base contains 414 time series, 203 of which are from ice-covered locations. The average time series contains six age-height pairs of data.

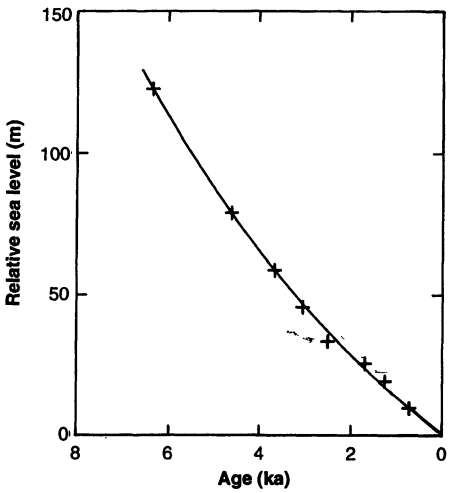

Fig. 2. The ^{14}C-controlled relative sea level curve for the Richmond Gulf of Hudson Bay (*15*) illustrating the exponential nature of the postglacial rebound that is observed at locations that were once ice covered. The relaxation time τ that characterizes the rebound at this site is 7600 years (longer than average for the Hudson Bay region), whereas the amplitude A is 96.2 m.

analyses of postglacial *rsl* histories with Eq. 2, I have assumed that C is time-independent. This is equivalent to assuming that the boundaries of the oceans are step discontinuities of amplitude sufficient to prevent everywhere inundation of the land by rising sea levels. In order to calculate paleotopography accurately it is necessary to calculate the time dependence of C as a part of the procedure that is used to determine $S(\theta,\lambda,t)$ from Eq. 2.

Assuming that the internal viscoelastic structure is known on the basis of first-stage inversions of the relaxation time observations (*16*), I used Eq. 2 to infer $I(\theta,\lambda,t)$ at the ice-covered points in the vicinity of which rebound time series are available. Tushingham and Peltier (*18*) used Eq. 2 in this way to construct an initial model, called ICE-3G, of the variation of ice cover since LGM on the basis of the assumption that $C(\theta,\lambda,t)$ was time-independent (not a serious restriction). Since this inversion, accurate new data on postglacial *rsl* change has become available. These data consist of measurements on samples from coral terraces for which accurate U-Th ages can be obtained (*5*) to fix the time scale. In developing the refined model ICE-4G based upon solutions at high spatial resolution to Eq. 2, I used these new data and explicitly incorporated the (exactly calculated) time dependence of $C(\theta,\lambda,t)$ that is required in the inference of paleotopography. In these analyses I assumed that the system was in a state of isostatic equilibrium at the LGM before the time melting commenced. That this assumption is reasonable, at least for the dominant Laurentide ice complex, follows from the observation that the characteristic relaxation time for the postglacial rebound of Laurentia is ~1500 years, based on most of the *rsl* data from this region [the example shown in Fig. 2 has the longest time scale of any time series in the data base]. Since more than 70% of LGM ice cover was in place by 31 ka and the remainder accumulated sufficiently rapidly thereafter that the complete load was in place at least 5000 years before the onset of deglaciation (*20*), the assumption of initial isostatic equilibrium should not introduce significant error. This does not of course imply dynamical equilibrium for the ice sheets themselves.

The function $S(\theta,\lambda,t)$ that is a solution to Eq. 2, given $I(\theta,\lambda,t)$ and a radial profile of mantle viscosity $\nu(r)$, is defined globally and represents the time-dependent separation between the geoid and the surface of the deforming solid Earth. That the history $S(\theta,\lambda,t)$ may be observed only when and where there is ocean does not detract from its global definition as an evolving geoid with respect to the surface of the solid Earth. At a typical ice-covered site with coordinates (θ,λ) the solution of Eq. 2 is a curve $S(\theta,\lambda,t)$ that goes through zero at LGM (when the system has yet to be perturbed from its initial state of isostatic equilibrium) and decreases monotonically to some negative level (T', say) at present. If the observed *rsl* curve from this site is such that present sea level corresponds to zero age, than the theoretical prediction $S(\theta,\lambda,t)$ is adjusted by adding $|T'|$ so as to force the curve to pass through zero (topography with respect to sea level) at present. The goodness of fit of this theoretical prediction to the observations is analyzed by investigating the misfit of $rsl(t)$ to $S(\theta,\lambda,t) + T'$. In this standard adjustment procedure lies the key to understanding how paleotopography may be inferred from the solution of Eq. 2. Because the globally defined solution $S(\theta,\lambda,t)$ is a prediction of first-order perturbation theory, the solution can be adjusted globally by the addition to $S(\theta,\lambda,t)$ of a time-independent field $T'(\theta,\lambda)$ that is chosen such that

$$S(\theta,\lambda,t_p) + T'(\theta,\lambda) = T_p(\theta,\lambda) \quad (4)$$

in which t_p is the present time and $T_p(\theta,\lambda)$ is the present topography with respect to sea level, and therefore a function that is zero only if the location (θ,λ) is at sea level, in which case the adjustment $T'(\theta,\lambda)$ is identical to that normally made in comparing solutions of Eq. 2 to $rsl(t)$-observations. This result immediately allows us to infer the topography of the rocky part of the planet with respect to sea level at all times from LGM to present as

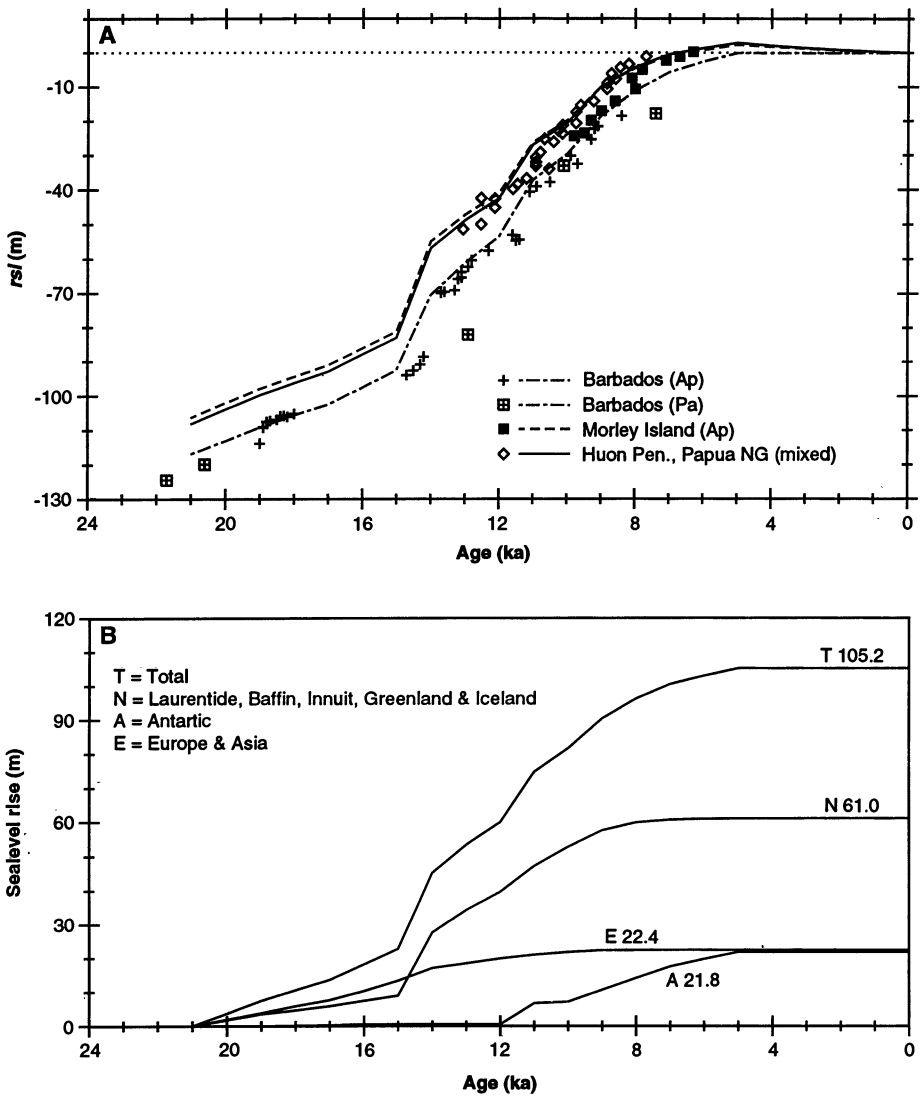

Fig. 3. (**A**) Comparison of the predictions of the ICE-4G model (denoted DIt-High Antarctic Ice tc distinguish it as a particular member of a closely related laboratory sequence generated by the process of iterative refinement) to the coral terrace–based observations at Barbados, Morely Island, and the Huon Peninsula of Papua New Guinea. (**B**) Disaggregation of the total eustatic (globally averaged) sea level rise delivered by the ICE-4G model (T) into North American (N), Eurasian (E), and Antarctic (A) components.

$T(\theta,\lambda,t) =$

$$S(\theta,\lambda,t) + [T_p(\theta,\lambda) - S(\theta,\lambda,t_p)] \quad (5)$$

The true paleotopography, including the contribution from the ice sheets of thickness $I(\theta,\lambda,t)$ is then

$$PT(\theta,\lambda,t) = T(\theta,\lambda,t) + I(\theta,\lambda,t) \quad (6)$$

Any time and place for which $PT(\theta,\lambda,t)$ is negative indicates the presence of ocean, whereas where $PT(\theta,\lambda,t)$ is positive there is (perhaps ice-covered) continent.

The full influence of time dependence of the ocean function $C(\theta,\lambda,t)$ can therefore be taken into account in the solution of Eq. 2 in an iterative fashion. I first fixed $C(\theta,\lambda,t) = C_p(\theta,\lambda)$ where $C_p(\theta,\lambda)$ is the present-day ocean function and then solved Eq. 2 to find a first guess for the paleotopography $PT^1(\theta,\lambda,t)$ from Eq. 6 and thus a next guess to the ocean function $C^1(\theta,\lambda,t)$. This procedure was repeated and typically yielded convergence in three iterations to an error tolerance of 3% in differential ocean area. In the results I present, Eq. 2 was solved iteratively in this way on a basis of spherical harmonics truncated at degree and order 512.

The ICE-4G Deglaciation History

The *rsl* histories predicted by the model for locations that were once covered by any substantial thickness of glacial ice are completely insensitive to variations of the ocean function. I therefore refined the ICE-3G deglaciation history by using a direct method to solve Eq. 2 as in (*18*). Here, however, the solution was constructed using the spherical harmonics methodology (*21*) rather than the finite element method. Aside from this methodological difference the main new data that I used to constrain better the melting history consists of the relative sea level history for Barbados that has recently been determined by Fairbanks (*20*) through the U-Th dating of coral terraces drilled from the flanks of the island in relatively shallow water. This record is of significantly higher quality than most of the ^{14}C dated *rsl* curves from sites that were once ice covered for two reasons. First, the U-Th dating on corals is significantly more precise than ^{14}C dating and second, and more importantly, the coral chronology extends back to LGM at 21 ka, whereas conventional *rsl* curves from ice-covered sites are seldom available from times before 8 ka. I therefore used the Barbados record both to calibrate the ^{14}C ages in the *rsl* data base (*5*) and to provide the primary global control on the deglaciation process.

The main characteristic of the Barbados *rsl* record that distinguishes it from other *rsl* curves for sites beyond the ice margins is that the record (Fig. 3A) clearly reveals two periods of relatively rapid sea level rise that bracket a period of more slowly rising sea level centered about 13 ka. The period of hiatus in the deglaciation process corresponds to the Younger-Dryas (Y-D) period of climate cooling that is well recorded in climate proxy data from Northwestern Europe. The period of rapid sea level rise following the Y-D is thought to be dominated by the disintegration of the Antarctic ice sheet (*18*). Because the marine ice sheets on the Barents and Kara seas are constrained to disappear rapidly following the LGM (*18*), the only viable source of the meltwater that is required to effect the rapid rise of sea level that precedes the Y-D is the Laurentian ice sheet that covered the northern half of the North American con-

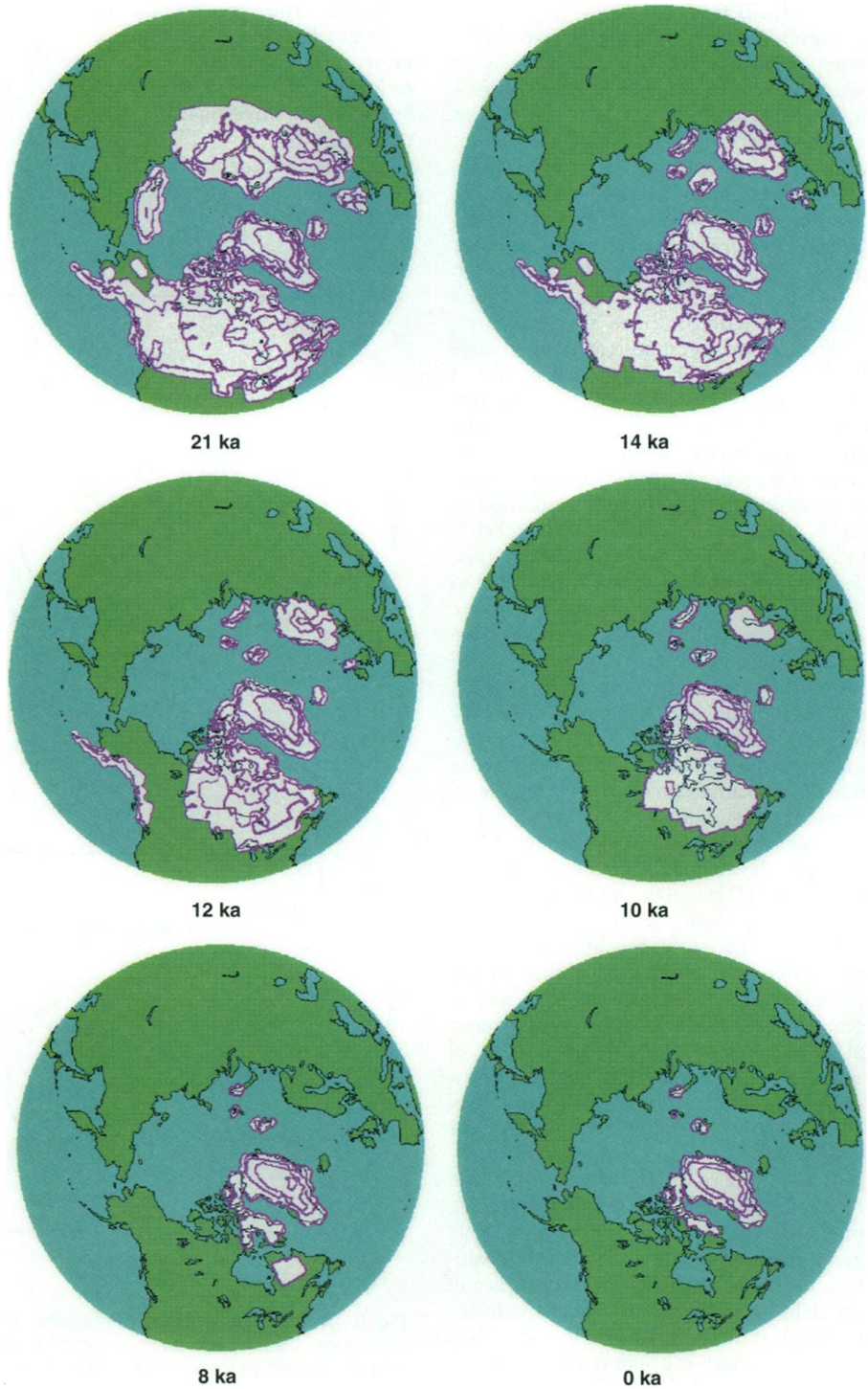

Fig. 4. Thickness isopachs for the ICE-4G model for a sequence of times beginning at Last Glacial Maximum at 21 ka and ending at the present. The contour interval is 1 km.

tinent. The main modification that I have made to the ICE-3G model in order to produce ICE-4G was therefore to incorporate a period of rapid Laurentide collapse, with the thickness history constrained to be nonzero only within the known locations of the evolving ice sheet margin (*10*). I also delayed slightly the melting history of this ice sheet thereafter. Also, the ICE-3G model had the Fennoscandian ice sheet too thin to extend over the mountains of northern Norway. It also had the centroid of the Barents Sea ice sheet too far south of Spitzbergen. Before settling on the ICE-4G model, I also tested the viability of a scenario in which a significant fraction of the total ice that was assumed in ICE-3G to have melted from Antarctica was shifted onto the Kara Sea, a thick Kara Sea ice sheet having often been suggested [discussed, for example, in (8)]. Because this ice is required to melt late in order to satisfy far field *rsl* data, the incorporation of such an event has a marked effect on some Northern Hemisphere *rsl* curves such as those from southern Sweden, which reveal a hiatus in rebound that correlates with the onset of Antarctic melting. This hiatus is not well explained by the scenario with a thick Kara Sea ice sheet and late deglaciation, and I therefore reject it as a plausible alternative to the significant Antarctic melting that is characteristic of the standard model.

The quality of the ICE-4G refinement to the deglaciation history as judged on the basis of the fit to the Barbados coral chronology is high (Fig. 3A). That this would be possible without violating the fits of the theoretical model to the *rsl* data from ice-covered sites was not clear a priori. The only significant misfits to the observations are near 7.5 ka and 13 ka and for the two oldest data points. Because these points all correspond to measurements on coral species (denoted PA on Fig. 3A) that may live at great depth below the sea surface, they therefore provide only a lower bound on sea level; thus, the misfits are unimportant. The high-quality data from Barbados are from samples of Aquapora Palmata (AP in Fig. 3A), because these corals live within 5 m of the sea surface. The slight phase lead of the model prediction compared to the observations at Barbados for the earliest period of rapid sea level rise is a consequence of the rather low temporal resolution at which the calculation is performed (1000 years) and is not indicative of an intrinsic problem with the inversion.

Although the quality of the fit to the Barbados data is high, the model has been tuned to obtain it; therefore, the fit might not be seen as surprising. However, the model so tuned equally well reconciles observations of *rsl* history in the west equatorial Pacific Ocean, for example at Morley Island (*22*) off the west coast of Australia and the Huon Peninsula of Papua New Guinea (*23*) (Fig. 3A). For the short record at Morley Island the age control is also based upon U/Th dating, whereas for the Huon Peninsula I have used the ^{14}C calibration of Bard *et al.* (*5*) to transfer the original ^{14}C ages to U/Th (essentially sidereal) ages. Inspection of Fig. 3A shows that the Huon data lie at systematically shallower depths than the Barbados data (by approximately 15 m at the same age), and the theoretical model tuned to fit Barbados accurately predicts this offset. The offset results because, following deglaciation, water was continuously siphoned from the equatorial oceans toward the poles (*21*), an effect that diminishes the net rise of sea level at Huon relative to the eustatic rise and increases it at Barbados. This redistribution of water over the ocean basins is required to ensure that the surface of the ocean (the geoid) is always coincident with a gravitational equipotential. Because of this dynamically driven redistribution of water, the *rsl* curve at Barbados does not provide a good approximation to the eustatic sea level curve but rather would lead to an overestimate of the amount of ice that melted during deglaciation if it were used to estimate the globally averaged (eustatic) sea level rise.

A central result is the net eustatic sea level rise delivered by the ICE-4G model, and the individual contributions to this history from its individual North American (including the Laurentian, Cordilleran, Innuitian, Greenland, and Iceland ice

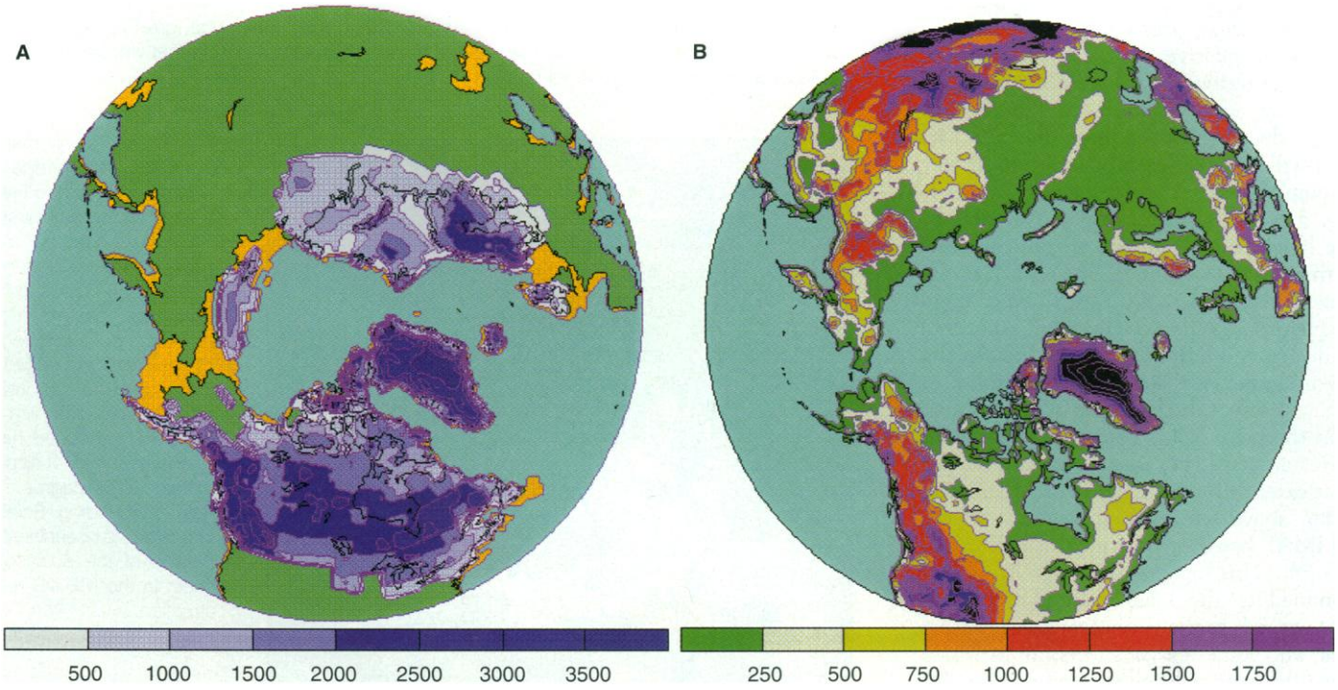

Fig. 5. Ice sheet height in meters relative to sea level at (**A**) glacial maximum and (**B**) present-day topography from a spherical harmonic expansion of the ETOPO5 data set to degree and order 512. In (A) the surface areas shown as beige are the regions that are now oceanic but were exposed land at LGM.

sheets), European (including the Scotland, Fennoscandian, Barents Sea, Kara Sea, and eastern Siberian ice sheets) and Antarctic components (Fig. 3B). The total model sea level rise is 105.2 m, an amount that is 57.8 m lower than the 163 m of the CLIMAP MAX model that has been used as the basis for past paleoclimate analyses. This marked diminution of ice amount clearly implies an equally marked diminution of ice sheet topographic height with respect to sea level, a principal boundary condition required in AGCM climate reconstructions.

The model deglaciation history implies that ice cover over both the Barents and Kara Seas disappeared rather early (Fig. 4). The Cordilleran ice sheet of western North America was the next major ice mass to disappear, and this is predicted to have occurred essentially by 12 ka. The maximum thickness of both the North American and Fennoscandian ice sheets was about 3 km, approximately 1.5 km less than the thickness of these ice sheets according to the CLIMAP MAX reconstruction. In order to convert these thicknesses accurately into topography with respect to sea level, however, the influence of the glacial isostatic depression of the Earth's surface under the weight of the ice load must be fully taken into account using the theory outlined in Eqs. 1 to 6.

Ice Age Paleotopography

The predictions of this topographically self-consistent theory consist of the time-dependent paleotopography $PT(\theta,\lambda,t)$ and the time-dependent ocean function $C(\theta,\lambda,t)$, aside from relative sea level $S(\theta,\lambda,t)$. Because the individual fields PT consist, to a first-order approximation, of the isostatically reduced thickness maps shown in Fig. 4, it will serve no useful purpose to display a complete sequence of these fields. Rather, Fig. 5 presents, in north polar projection, the height of the surface of the ice sheets with respect to sea level at LGM, and the present-day topography $T_p(\theta,\lambda)$ based upon a spherical harmonic expansion truncated at degree and order 512 that is used in the theory to define the $T'(\theta,\lambda)$ field in Eq. 4. Comparison of the two parts of Fig. 5 shows that the present-day Hudson Bay lowlands were, at LGM, covered by Laurentian ice that extended to a height of approximately 2 km above sea level, in contrast to the CLIMAP-based reconstructions of close to 3.5 km. This topographic difference is not confined to the Laurentian platform but also extends to the Fennoscandian, Barents Sea, and Kara Sea ice sheets, all of which have similarly reduced topographic heights above sea level with respect to the CLIMAP MAX reconstruction.

Of similar importance to the paleotopographic relief of the ice sheets themselves insofar as the understanding of past climate regimes is concerned, is the variation through time of the surface area of the planet that is covered by ocean. This is because of the marked difference in surface heat capacity between water and land. The variation of ocean area through time is captured by the time-dependent ocean function. As shown in Fig. 6, several of the land bridges that existed at LGM, between Alaska and Asia (the continent of "Beringia"), between France and Britain, and between Australia and New Guinea, disap-

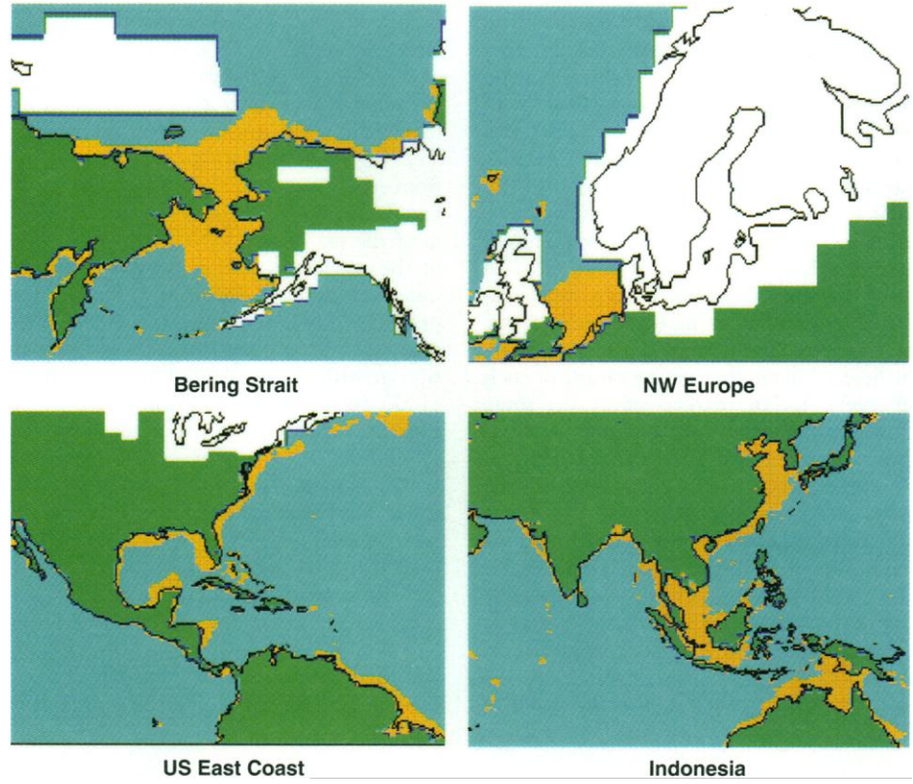

Fig. 6. Net change in the ocean function from LGM to present for the four geographic regions shown on the individual plates. As in Fig. 4, the regions shown as beige are those that were exposed land at LGM but which are now covered by ocean.

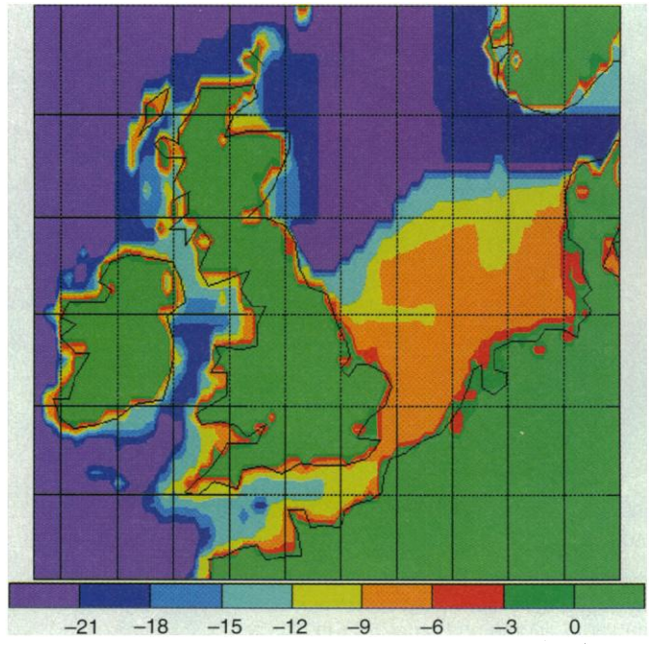

Fig. 7. Inundation map for the LGM land bridge that connected Britain to France at LGM shown previously on Fig. 5. The color bar at the base of the map denotes the time, in thousands of years ago, that each geographical point on the land bridge was inundated by the ocean. The computation on the basis of which this map was produced had a spatial accuracy of approximately 0.25 degree. The halo surrounding Scotland indicates the oceanward extension of the Scottish ice sheet in the ICE-4G reconstruction.

peared as sea level rose in response to the collapse of LGM ice sheets. Also apparent is that vast expanses of continental shelf off the east coasts of North America and South America, off the east coast of China, and through the Indonesian Archapelago were exposed at LGM. These regions are likely to have been important sources of terrigeneously derived atmospheric dust that are known to have been characteristic of the full glacial climate state (*24*).

The time-dependent ocean function is important not only because variations in the surface area covered by ocean are climatologically important but also because theoretical predictions of the time that an LGM land bridge becomes covered by water may be evaluated geologically. Typically, this horizon is marked in a core drilled in the modern sea floor but a peat layer that may be dated with the ^{14}C method (*25*). Because the inundation horizon typically develops much earlier than the end of the deglaciation process, such data will prove extremely useful in further constraining the theoretical model. As an example, I show in Fig. 7 a map of the predicted age of the inundation horizon for the land bridge that joined England to France at LGM. The model predicts that the land bridge was inundated from 21 ka to 6 ka and that the exterior of the bridge became water-covered during the first of the two periods of rapid melting that bracket the Younger Dryas, while the rest was inundated during and subsequent to the most recent of these periods.

Ice Age paleotopography is an important boundary condition that is required in the use of AGCMs for the reconstruction of past climates. Inferences of this topography using postglacial *rsl* data from ice-covered regions have established that the CLIMAP model of this topography that has been used in previous analyses of this kind was excessive. In terms of global sea level equivalent ice volume, the preferred CLIMAP MAX model suggested that the glacial-interglacial transition involved a eustatic sea level rise of 163 m. The ICE-4G model deduced here can accommodate an eustatic *rsl* rise of only 105.2 m. The 55% excess ice in the CLIMAP reconstruction implies that there are substantial differences of ice sheet topographic height with respect to sea level and these differences will lead to significant differences in LGM to present climate states that will be inferred on the basis of AGCM experiments [for example, as might be suggested by (*2*)]. A new sequence of such experiments is currently under way internationally in the context of the Paleoclimate Model Intercomparison Project (PMIP), which is a major activity of the PAGES (Past Global Changes) core project of the IGBP (the International Geosphere-Biosphere Programme). These experiments will use the ICE-4G model.

REFERENCES AND NOTES

1. S. Manabe and J. A. Broccoli, *J. Geophys. Res.* **90**, 2167 (1985); J. Kutzbach and P. J. Guetter, *J. Atmos. Sci.* **43**, 1726 (1986); D. Rind, *J. Geophys. Res.* **92**, 4241 (1987); M. Lautenschlager and K. Herterich, *ibid.* **95**, 22,547 (1990); S. Joussaume, *ibid.* **98**, 26 (1993).
2. E. J. Barron and W. H. Peterson, *Science* **244**, 684 (1989).
3. N. J. Shackleton, A. Berger, W. R. Peltier, *Trans. R. Soc. Edinburgh Earth Sci.* **81**, 251 (1990).
4. W. S. Broecker and J. van Donk, *Rev. Geophys. Space Phys.* **8**, 169 (1970); J. Imbrie *et al.*, *Paleoceanography* **8**, 699 (1993).
5. E. Bard, B. Hamelin, R. G. Fairbanks, A. Zindler, *Nature* **345**, 405 (1990).
6. COHMAP Members, *Science* **241**, 1043 (1988).
7. CLIMAP Project Members, *ibid.* **191**, 1131 (1976); *Geol. Soc. Am. Map Ser. MC-36* (1981).
8. G. H. Denton and T. Hughes, *The Last Great Ice Sheets* (Wiley, New York, 1981).
9. J. Imbrie and N. G. Kipp, in *Late Cenozoic Ice Ages*, K. Turehian, Ed. (Yale Univ. Press, New Haven, CT, 1977), pp. 71–181.
10. V. K. Prest, *Geol. Surv. Can. Pap. 84-10* (1984); *Geol. Surv. Can. Map 1584A* (1984); A. S. Dyke and V. K. Prest, *Geol. Surv. Can. Map 1702A* (1987); *Geol. Surv. Can. Map 1703A* (1987).
11. W. R. Peltier, *Rev. Geophys. Space Phys.* **12**, 649 (1974); ——— and J. T. Andrews, *Geophys. J. R. Astron. Soc.* **46**, 605 (1976); W. R. Peltier, *Adv. Geophys.* **24**, 1 (1982); *J. Geophys. Res.* **90**, 9411 (1985); in *Mantle Convection*, W. R. Peltier, Ed. (Gordon and Breach, New York, 1989), pp. 389–478.
12. P. Wu and W. R. Peltier, *Geophys. J. R. Astron. Soc.* **76**, 202 (1984).
13. W. R. Peltier, R. A. Drummond, A. M. Tushingham, *ibid.* **87**, 79 (1986); J. X. Mitrovica and W. R. Peltier, *Geophys. Res. Lett.* **18**, 235 (1991); W. R. Peltier, A. M. Forte, J. X. Mitrovica, A. M. Dziewonski, *ibid.* **19**, 1555 (1992).
14. A. M. Tushingham and W. R. Peltier, *J. Geophys. Res.* **97**, 3285 (1992).
15. C. Hillaire-Marcel, in *Earth Rheology, Isostasy and Eustasy*, N. A. Mörner, Ed. (Elsevier, Amsterdam, 1980), pp. 215–230.
16. W. R. Peltier, *Geophys. J. R. Astron. Soc.* **46**, 669 (1976); J. X. Mitrovica and W. R. Peltier, *Geophys. J. Int.* **104**, 267 (1991); *ibid.* **114**, 45 (1993); in preparation.
17. P. Wu and W. R. Peltier, *Geophys. J. R. Astron. Soc.* **74**, 377 (1983).
18. A. M. Tushingham and W. R. Peltier, *J. Geophys. Res.* **96**, 20053 (1991); *ibid.* **97**, 3285 (1992).
19. W. R. Peltier, W. E. Farrell, J. A. Clark, *Tectonophysics* **50**, 81 (1978).
20. R. G. Fairbanks, *Nature* **342**, 637 (1989); James L. Rubinstone and Richard G. Fairbanks, in preparation.
21. W. R. Peltier, *Geophys. J. R. Astron. Soc.* **A6**, 669 (1976); J. X. Mitrovica and W. R. Peltier, *J. Geophys. Res.* **96**, 20053 (1991).
22. A. Eisenhauer *et al.*, *Earth Planet. Sci. Lett.* **114**, 529 (1993).
23. J. Chappell and H. Polach, *Nature* **349**, 147 (1991).
24. M. De Angelis, N. I. Barkov, V. N. Peterov, *ibid.* **325**, 318 (1987).
25. S. A. Elias, S. K. Short, R. L. Phillips, *Quat. Res.* **38**, 371 (1992).
26. R. A. Shinn and E. J. Barron, *J. Geophys. Res.* **94**, 151 (1989).
27. The topographic data sets derived from the theoretical analyses have been produced at 1000-year intervals beginning from 21 ka and continuing to the present. They are now on file in digital format at the World Data Center A for Palaeoclimatology, which is a part of the National Geophysical Data Center in Boulder, CO. These data are accessible via internet under FTP/PALEO/PMIP via anonymous@NGDCC1.NGDC.NOAA.GOV. The author would appreciate feedback from users of these data at PELTIER@RAINBOW.PHYSICS.UTORONTO.CA.

28. I thank J. Anderson, J. Andrews, W. Blake, G. Boulton, G. Denton, A. Dyke, R. Fairbanks, J. Fastook, S. Forman, S. Funder, M. Grosswald, J. Imbrie, J. Klemen, R. Lagerback, S. Lehman, L. Polyak, V. Prest, M. Punhari, W. Ruddiman, A. Solheim, and D. Sugden, who contributed critical analyses of the previous ICE-3G reconstruction that led to this refinement. I also thank R. Drummond for assistance, the Natural Sciences and Engineering Research Council of Canada for continuing support via grant A9627, and the NOAA Climate and Global Change Program. The ideas developed in this paper were originally presented at a special Union Symposium at the winter 1993 meeting of the American Geophysical Union that was held in honor of Bill Kaula.